J Mater Sci (2008) 43:368–377
DOI 10.1007/s10853-006-1314-y

Thermoelectric properties of porous zinc oxide ceramics doped with praseodymium

Yoshihiro Inoue · Yoichi Okamoto · Jun Morimoto

Received: 9 November 2005 / Accepted: 22 November 2006 / Published online: 17 October 2007

Abstract We evaluated praseodymium (Pr) doping effects on thermoelectric properties of porous zinc oxide (ZnO) ceramics. The low density ceramics composed of ZnO and an additive of Pr (0.5 and 0.1 mol%) oxide were prepared by sintering processes in different atmospheres (air and oxygen), where the additives were Pr_6O_{11} known for phase transformations and the trioxide Pr_2O_3 with low valence state different from Pr_6O_{11}. Thermoelectric properties of the samples were measured between 313 K and 903 K. At high-temperature around 590 K, some samples showed a maximum of electrical resistivity. We discussed the origin of the maximum on the basis of carrier transport model on gas sensor and varistor. From the results, The maximum appearance was attributable to an interchange of carriers through defects complex closely related with enhanced zinc vacancies acceptor-like in the vicinity of grain boundaries (GB), where the defect complex seemed to be caused by Pr with valence state between 3+ and 3.78+ around GB. The doping Pr into ZnO matrix is expected to be advantageous to improve thermoelectric power.

Introduction

Versatile zinc oxide (ZnO) has attracted a great deal of interest because of a material for piezoelectric transducers, chemical gas sensing devices and so on [1, 2]. In particular, ZnO varistor ceramics with additives such as praseodymium (Pr) and cobalt (Co) oxide have come into practical use [3, 4]. The nonlinear current–voltage (I–V) characteristics of varistors are well explained by the double Schottky barrier (DSB) model based on the interfacial acceptor state. Nowadays, the work is proceeding with application of unique properties of ZnO to UV-blue optical devices, transparent electrodes and thin film transistors [5–8]. Because, ZnO is one of direct transition semiconductors with a wide energy band gap of about 3.3 eV, high carrier mobility and high transparency at room temperature. However, contrary to the remarkable application, the native defects in ZnO and the functionalities still have been in controversy. For example, the subjects of luminescence originating in native defects, origins of interfacial acceptor level in the varistor, and point defects complex related with dopants as well as native defects are argued. As for native defects, they are considered as zinc interstitial (Zn_i), oxygen interstitial (O_i), zinc vacancy (V_{Zn}), oxygen vacancy (V_O), and these complex [9–11].

Recently, it has been reported that the hydrogen in ZnO forms a shallow donor level, and then the hydrogen is the one of primary origins of *n*-type conductivity in as-grown ZnO [12, 13]. Furthermore, the followings are suggested by first-principles pseudopotential method; the V_{Zn} is associated with intrinsic green luminescence, and the Zn_i or the zinc antisite contributes to *n*-type conductivity of intrinsic ZnO [14–16]. For varistors of ZnO-Pr-Co system, Oba et al., have reported that the formation of acceptor-like native defects is associated with the presence of Co dopants which play an important role for generating interfacial acceptor states, and there is the dominance of V_{Zn} over other oxygen excess defects in the vicinity of grain boundaries (GB) [17, 18]. Additionally, the V_{Zn} is produced by Pr just around GB [19]. Hence, the nonlinear I–V

Y. Inoue (✉) · Y. Okamoto · J. Morimoto
Department of Materials Science and Engineering,
National Defense Academy, 1-10-20 Hashirimizu, Yokosuka
239-8686, Japan
e-mail: f05005@nda.ac.jp

characteristic can be attributed to V_{Zn} with acceptor-like electronic states in the Pr-doped grain boundary [20]. It has been also reported by many researchers that the acceptor state is related with both the excess oxygen and oxygen-ion adsorbed on the grain surface (GS) and the GB [21–23]. Furthermore, the origin of nonlinear I–V characteristic have been confirmed in porous ZnO ceramics doped with Al_2O_3 as well as non-doped ZnO ceramics under various oxidizing conditions [24, 25]. The explanation and discussion about the characteristic is based on the models of gas sensor reaction [24, 25], where the change of electrical resistivity ρ is caused by the carrier transport through the chemical reaction between absorbed or diffused oxygen ion (O^-, O^{2-}, and so on) and ambient gas.

Evaluating the electrical characteristic originating in native defects on ZnO is important to a modification in ZnO-related devices. Furthermore, it is interesting that the thermoelectric properties of porous ZnO ceramics doped with Pr are studied on the improvement in thermoelectric power. In this study, the porous ZnO ceramics with different Pr doping conditions were prepared by a simple sintering procedure in air and oxygen atmosphere. The low density bulks were composed of ZnO and an additive which was one of two kinds of Pr oxides. One is Pr_6O_{11} known for phase transformations [26, 27] and the other is the trioxide Pr_2O_3 with lower valence state than that of Pr_6O_{11}, where the Pr content were 0.5 mol% and 1 mol%. The thermoelectric properties of samples, that is, both the temperature dependence and the heat-treatment cycle dependence of ρ and Seebeck coefficient α were measured between 313 K and 903 K in reducing atmosphere. Some samples showed a unique common characteristic, that is, a maximum of ρ at high temperature around 590 K. Thus, we try to explain and discuss the unique characteristic in view of the defect-related complex in the porous ZnO:Pr ceramics based on varistors and gas sensors as well as native defects in intrinsic ZnO. We also discuss the application of a sample with the highest thermoelectric potential to electrical and electronic field from the aspect of the potentiality and the stability in heat-treatment cycle.

Experimental procedure

Starting materials for ZnO:Pr ceramics were ZnO powders (99.99% purity, Kojundo Chemical Lab Co. Ltd.), Pr_2O_3 powders (99.9% purity, Kojundo Chemical Lab Co. Ltd.) and Pr_6O_{11} powders (99.9% purity, Kojundo Chemical Lab Co. Ltd.). For precursor mixed powders, both the Pr_2O_3 and the Pr_6O_{11} powders were weighed as 0.5 and 1 mol% for Pr content in the final mixed powders including ZnO, and weighed powders were mixed in an agate mortar for 1 h. Such final four kinds of mixed powders and ZnO only powders were placed in a die 20 mm in diameter and then pressed at 100 MP at room temperature. The obtained uniaxial pressing pellets were sintered in air and oxygen atmosphere at 1023 K for 5 h, here the heating and cooling rate for sintering was 5 K/min. The sintered samples about 2 mm in thickness were cut into square plates (about 10 mm × 10 mm). Crystal phases of sintered samples were characterized by X-ray powder diffraction (XRD) analysis using XRD system with Cu Kα radiation accelerated at 40 kV and 40 mA, where, we used the pre-ground samples which were fully converted in a powdery state in an agate mortar. Furthermore, to confirm porous state, we observed a fractured surface by scanning electron microscope (SEM).

The ρ and α of samples were measured between 313 K and 893 K in an infrared image furnace filled with flowing nitrogen gas. Here, a square sample was fixed on the cupper stage with thermocouple by using silver pastes and then attached to electrodes. The temperature dependences of ρ and α were simultaneously measured by conventional DC four-terminal method and conventional DC method, where the sample was heated and cooled at the rate of 10 K/min with temperature difference over 10 K at both ends of the sample kept. A combination process of both a heating and a cooling can be counted as one-cycle for heat-treatment. Thus, we repeated this cycle through 9 times in all. However, the first cycle was performed without measurement. Because the obtained data in first-cycle included errors on the ground that silver paste was not completely burned in the sample and the electrodes. Hence, ρ and α were measured over 2nd-cycle and then the cycle for the measurement were repeated 8 times.

Results and discussion

Structural properties for samples

As the result of XRD measurement, the obtained samples doped with Pr showed the XRD patterns of ZnO crystal including Pr oxide crystals. Figure 1 shows typical XRD patterns for samples doped with 1 mol% Pr (Pr_2O_3 and Pr_6O_{11}) and nothing sintered in air, where the characters of AZP21, AZP61, and AZN represent the samples, respectively. For the samples doped with Pr_2O_3, the segregated Pr oxide phase was only Pr_6O_{11} phase, and then the differences in XRD intensities among the samples were shown. Samples doped with Pr_6O_{11} showed the XRD peaks of Pr_6O_{11} phase and PrO_2 phase in addition to weak peaks which are probably identified with Pr_4O_7 phase, and then the differences in XRD intensities were also shown. To comprehend the structural characteristics and the segregations of each as-sintered sample, we summarize the result

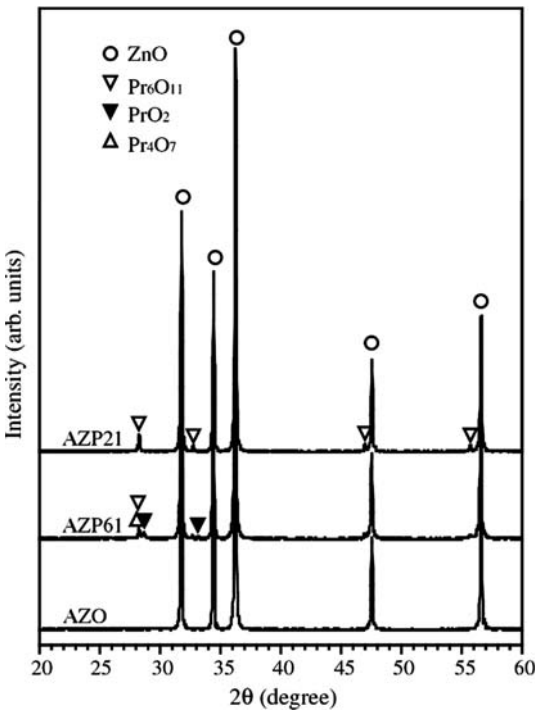

Fig. 1 Typical XRD patterns for AZP21, AZP61 and AZO

of XRD measurement in addition to samples name, lattice parameters which were averaged and estimated from angle of 2θ for XRD peaks of ZnO (101) and ZnO (102) and the ratio of XRD intensity of Pr_6O_{11} (111) (and PrO_2 (111)) to that of ZnO (101) in Table 1. Here, we can notice that the both of Pr oxides precursor are oxidized, and the degree of segregation varies according to sintering atmosphere except for samples of AZP21, OZP21, AZP605 and OZP605. However, we can find that the apparent difference in the lattice parameters for ZnO is not seen among all samples and there is a little contraction of ZnO crystal lattice in OZP25. As for the composition of samples, there is a possibility of changing before and after sintering because some additives and ZnO might be evaporated during sintering. However, in view of the comparisons between samples, the accurate composition of samples seems not to be so important in this study due to the large difference of 0.5 mol% in Pr content.

Typical SEM images of a fractured surface of samples of AZP205, OZP205, AZP61, OZP61, AZN, and OZN are shown in Fig. 2(a–f), respectively. In all samples, a pore is not seen on the GS although there are many gaps as shown in Fig. 2. In Fig. 2(b, e), the grain growth of OZP205 and AZN seems to be enhanced than that of the others. However, we could not confirm the dependence of grain growth originating in the difference of Pr content, additive kinds, and sintering atmosphere in this work. The difference of grain growth in our samples might be given rise to pressing conditions with lack of homogeneous compression. Although an evident GB layer and segregations at the triple point are often reported in surface images of ZnO varistor with high density and grain growth enhanced, such characteristics are not seen in our obtained SEM images. Hence, our samples have the porous state, that is, the lower density than that of commercial varistors.

Temperature dependence of electrical resistivity

Samples doped with Pr_2O_3

The temperature dependence of ρ in 2nd and 9th of cycle for AZP205, OZP205, AZP21 and OZP21 are shown in Fig. 3(a–d), respectively. Here, _2up, _2down, _9up and _9down represented by characters indicate the heating process in 2nd-cycle, the cooling process in 2nd-cycle, the

Table 1 The results of XRD analysis are summarized: the additive, Pr content, sintering environment, samples name, lattice constant for ZnO (*a*-axis and *c*-axis) and ratio of XRD intensity (Pr_6O_{11} (111) and PrO_2 (111))

Additive	Pr content (mol%)	Sintering environment	Samples name	Lattice constant for ZnO		Ratio of XRD intensity[a]	
				a-axis (nm)	*c*-axis (nm)	Pr_6O_{11}(%)	PrO_2 (%)
Pr_2O_3	0.5	air	AZP205	0.3246	0.5203	2.2	–
		oxygen	OZP205	0.3247	0.5201	1.5	–
	1	air	AZP21	0.3246	0.5203	4.6	–
		oxygen	OZP21	0.3250	0.5203	4.6	–
Pr_6O_{11}	0.5	air	AZP605	0.3247	0.5204	0.3	1.0
		oxygen	OZP605	0.3250	0.5203	0.3	0.9
	1	air	AZP61	0.3249	0.5204	1.9	1.5
		oxygen	OZP61	0.3248	0.5203	0.3	2.5
non	0	air	AZN	0.3251	0.5204	–	–
		oxygen	OZN	0.3250	0.5205	–	–

[a] XRD intensity for ZnO (101) plane = 100%

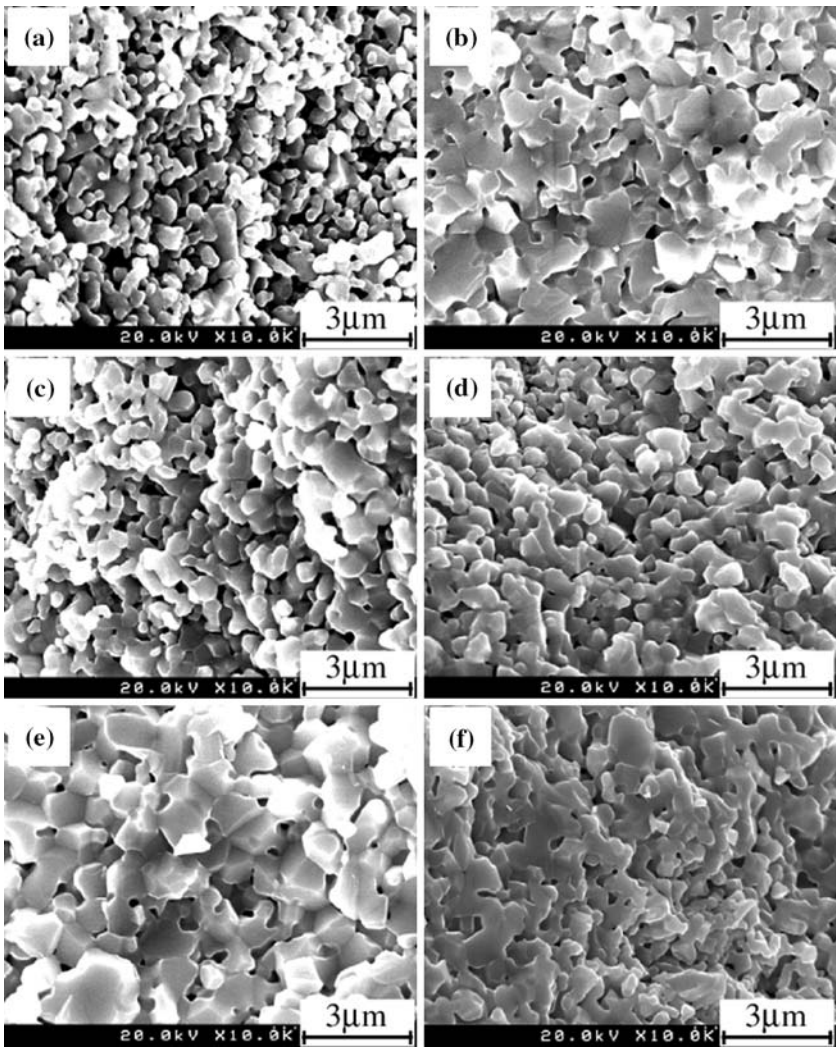

Fig. 2 SEM images of fracture surface of (**a**) AZP205, (**b**) OZP205, (**c**) AZP61, (**d**) OZP61, (**e**) AZN and (**f**) OZN

heating process in 9th-cycle and the cooling process in 9th-cycle, respectively. As shown in Fig. 3, all samples show the thermal hysteresis and the maximum of rho between 500 K and 667 K.

Compared the maximum of OZP21_9up in Fig. 3(d) with that of OZP205_9up in Fig. 3(b), the increasing of ρ with increasing temperature in OZP21_9up is also larger than that in OZP205_9up in the same manner as the relationship between AZP205_9up and AZP21_9up.Furthermore, compared the temperature dependence of samples sintered in air as shown in both Fig. 3(a, c) with that of samples sintered in oxygen as shown in both Fig. 3(b, d), there is a critical difference in temperature coefficient of ρ between 333 K and 500 K. The former inclines to the negative temperature coefficient (NTC) and the latter inclines to the positive temperature coefficient (PTC). Moreover, for 9th-cycle of all samples doped with Pr_2O_3, the consistency of ρ is seen in lower temperature range.

Non-doped samples

The temperature dependence of ρ in 2nd and 9th of cycle for AZN and OZN are shown in Fig. 3(a, b), respectively. In Fig. 4(b), the thermal hysteresis of rho for OZN is also obviously different from that for AZN as shown in Fig. 4(a).

For both AZN and OZN, they have no maximum of ρ and then indicate semiconductor-like behavior that ρ decreases with increasing temperature. Hence, the total lower ρ of AZN seems to be due to the high carrier concentration in as-sintered ceramics, and the larger change of ρ for OZN in the whole range implies that as-sintered ceramics can have many acceptor-like defects [9–11, 24, 25]. The sintering process in oxidizing atmosphere can have an impact on electrical properties of ZnO. Furthermore, the fact that ρ of OZN suddenly decreases between 500 K and 667 K, where the maximum of ρ appears in

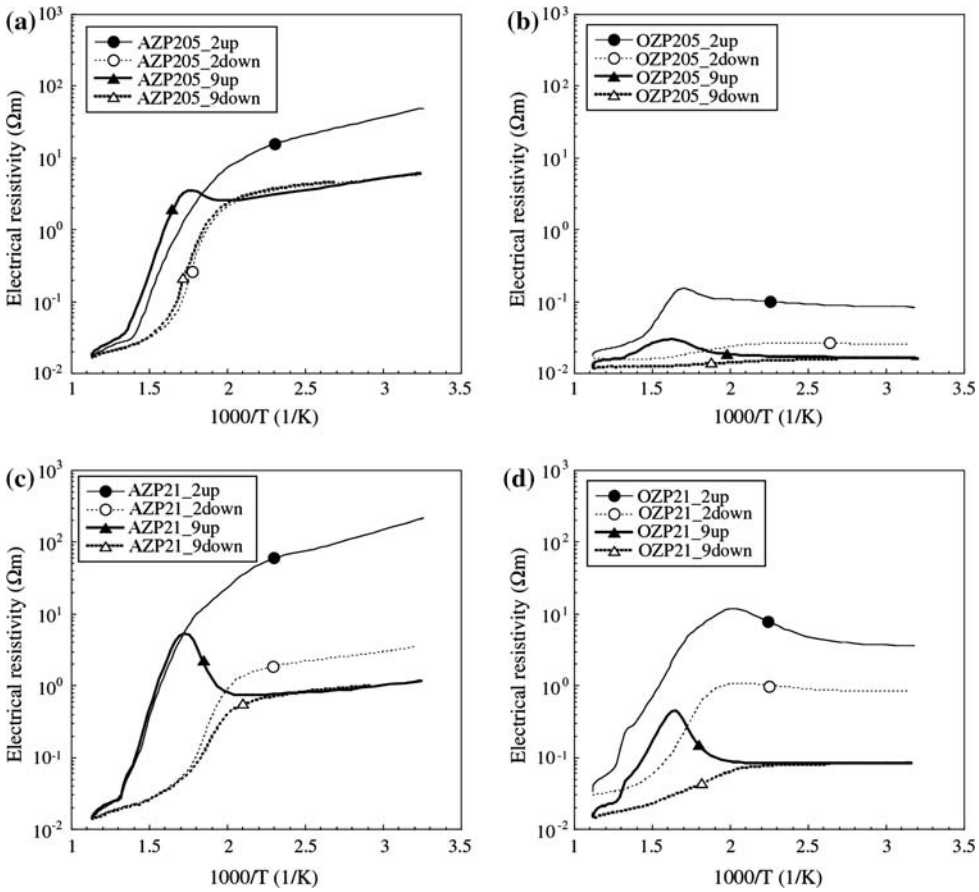

Fig. 3 The temperature dependence of ρ at 2nd-cycle and 9th-cycle for (**a**) AZP205, (**b**) OZP205, (**c**) AZP21 and (**d**) OZP21

samples doped with Pr_2O_3, suggests that the carrier transport mechanism in Pr doping samples and in non-doped ZnO is intimately related to each other. The origin of carrier transport mechanism is closely related with acceptor-like defects in the vicinity of GB [17–23]. If the maximum of rho in Pr doping samples is associated with the acceptor-like defects in ZnO, the effect of Pr doping might be the enhancement of V_{Zn} in the vicinity of GB [19].

On the other hand, the lower ρ is also confirmed for OZP205 as well as AZO. In Fig. 2, these AZO and OZP205 were composed of larger grains than others. It means that both AZO and OZP205 had lower porosity than others. Takata et al., have measured ρ with extremes of ZnO doped with Al_2O_3 in air and under reduced pressure in the range from 303 K and 953 K as a function of the degree of sintering, and report that extremes become attenuated and the activation energy for the low-temperature region decreased as the degree of sintering increased [24]. Thus, the lower ρ of both AZO and OZP205 might be also caused by the grain growth.

Takata et al., also explains the experimental data in terms of the effects of the microstructure of the ceramics and the chemisorbed oxygen [24]. In Subsect. ''Samples doped with Pr_2O_3'', we pointed out that the difference of sintering atmosphere determined the type of NTC and PTC in lower temperature region. Hence, we can explain the relationship of the experimental data and the grain microstructure associated with chemisorbed (and diffused) gases. The change of ρ should be attributable to different concentrations of chemisorbed (and diffused) gases on GS, in the vicinity of GB and grain-interior in terms of the gas sensor model [24, 25]. Moreover, the different concentrations of such gases should be also attributable to the state of defects on GS and so on [21–23] Here, the considerable defects can be regarded as donor-like defects, acceptor-like defects and chemisorbed gases [9–11, 21–25]. As for the effects of heat-treatment in nitrogen atmosphere, both the doping samples sintered in air and oxygen exhibit that ρ of 2nd-cooling stage is much lower than that of 2nd heating stage, whereas the non-doped samples does not exhibit. The performance of heat-treatment in nitrogen flow largely affects electrical properties of samples doped with Pr_2O_3 in an early stage in particular. This means that the chemical reactions should be initiated on GB, GS, the vicinity of GB, grain-interior and so on.

Furthermore, it is reported that the heat-treatment in reducing atmosphere can trigger the degradation of ZnO varistor [28, 29], and then the origin of degradation is

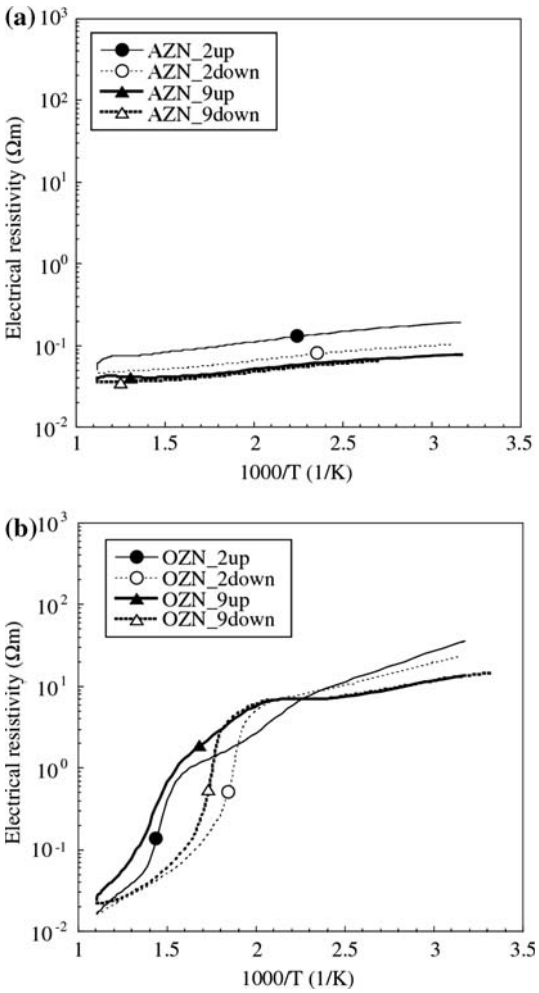

Fig. 4 The temperature dependence of ρ at 2nd-cycle and 9th-cycle for (**a**) AZN and (**b**) OZN

related with the collapse of DSB because of the release of chemisorbed gases [30, 31] and reaction with H_2O [32, 33]. In our case, it is just conceivable that the change of ρ is caused by chemical reaction on GB and so on through such the degradation. In terms of thermal degradation of varistor, it has been also suggested that the degradation needs the following two gas diffusion mechanisms of greatly differing rate; GB diffusion of oxygen or lattice defects is the slower mechanism, and gas diffusion through macroscopic flaws, such as micro cracks or interconnected pores, is the faster mechanism [34]. In our case, as for the chemical reaction on GB and so on, the following two remarkable aspects can be considered; one is that chemisorbed gases or released gases are exposed to porous space surrounded by grains (GB and the vicinity of GB) inside the bulk, and the other is that such gases are exposed to ambient outside the bulk. Such aspects can affect the carrier concentration and the carrier mobility around GB, and thus govern the total ρ.

In Figs. 3 and 4, all samples show a concordance of the value and the change of ρ at 9th-cycle in lower temperature range, while the maximum of ρ remains in higher temperature region even though the heat-treatment is repeated many times. This indicates that the chemical reaction inside and outside the bulk in lower temperature region are steady or in equilibrium. Hence, the maximum of ρ should be closely related with the effects of an additive, that is, existences of Pr in vicinity of GB. For ZnO-Pr-Co system varistor, it have been reported that ZnO grains are three-dimensionally separated from the intergranular Pr oxides [35, 36]. Here, the phase transformation from fcc-Pr_6O_{11} into Pr_2O_3 was confirmed when the sintering temperature increased over 1650 K. Moreover, Wakiya et al., reported that the redox reaction of Pr oxide in the ZnO grains is strongly affected by the microstructure, where the Pr_2O_3 phase in the ZnO matrix remains as a stable phase[37]. For the reasons mentioned above, the carriers are probably transported between porous space and grains including the vicinity of GB inside the bulk, and between grains on the vicinity of bulk surface and ambient gases outside the bulk.

Samples doped with Pr_6O_{11}

The temperature dependence of ρ in 2nd and 9th of cycle for AZP605, OZP605, AZP61 and OZP61 are shown in Fig. 5(a–d). The temperature dependence of ρ for both AZP605 and AZP61 as shown in Fig. 5(a, c) shows the same tendency of that for samples doped with Pr_2O_3 as shown in Fig. 3. However, there are differences in Pr content dependence of ρ maximum. The degree of the ρ increase at maximum for samples doped with Pr_2O_3 is larger than that for Pr_6O_{11} doped samples. The temperature dependences of ρ for both OZP605 and OZP61 are much different from that for the other samples although the PTC of ρ is shown in lower temperature range. In particular, there is no-maximum of ρ as shown in the other samples between 500 K and 667 K. We can exclude both OZP605 and OZP61 as the exception from the point of view mentioned above. These samples seem to have the electrical properties different from that of the others. In Table 1, it is obvious that both OZP605 and OZP61 as-sintered ceramics include a few segregated phases composed of Pr_6O_{11}, PrO_2 and uncertain Pr_4O_7. Here, uncertain phase may be the complex composed of PrO_x with defect fluorite structure originating in multi phase transformations [26, 27].

For Pr doped ZnO ceramics (P–ZnO), Ohashi et al., reported that both effective charge of Pr-ion and crystalline form of PrO_x are changed with oxygen partial pressure [38]. The chemical state of PrO_x as well as the coordination structure in GB region are modified by thermal treatment. Then, Pr-ion tends to be easily reduced in P–ZnO than in

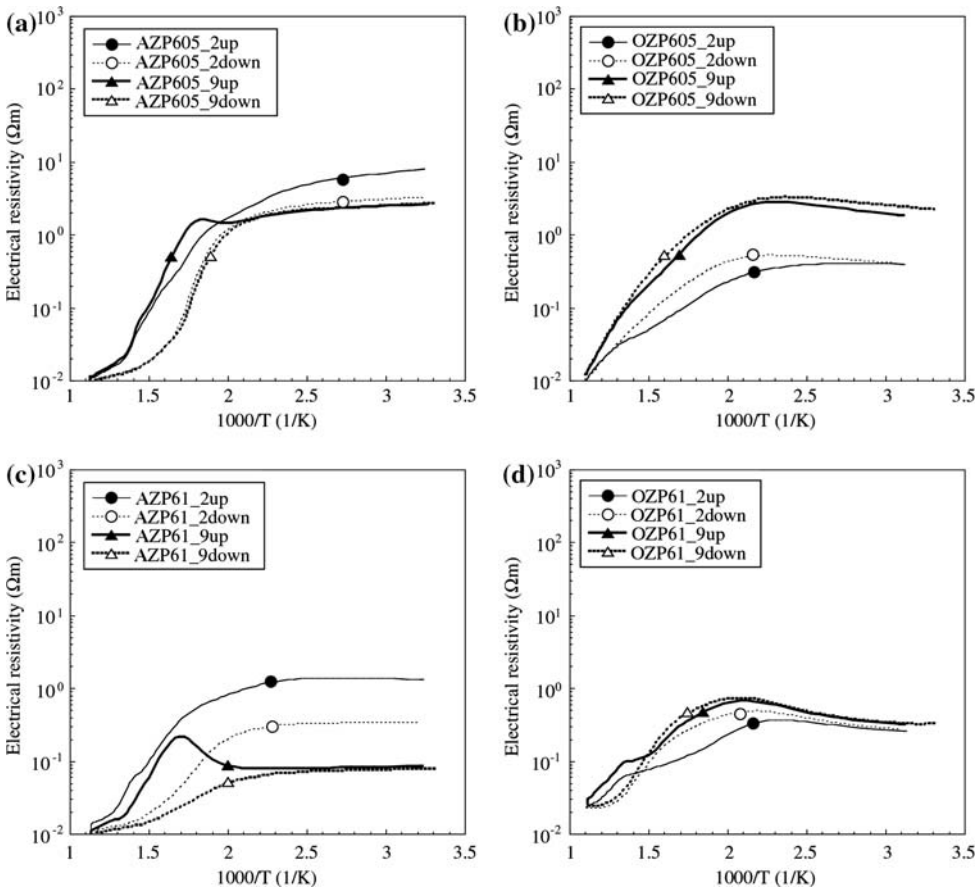

Fig. 5 The temperature dependence of ρ at 2nd-cycle and 9th-cycle for (**a**) AZP605, (**b**) OZP605, (**c**) AZP61 and (**d**) OZP61

pure PrO_x. Reference [38] allows us to get the correspondence between x in PrO_x and n in Pr^{n+} by using Fig. 4 in Ref. [38]. For example, $PrO_{1.5}$ (Pr_2O_3) is $Pr^{3.0+}$, $PrO_{1.75}$ (Pr_4O_7) is $Pr^{3.5+}$, $Pr0_{1.83}$ (Pr_6O_{11}) is $Pr^{3.78+}$, and $PrO_{2.0}$ (PrO_2) is $Pr^{4.0+}$, respectively. Thus, in case of samples doped with Pr_2O_3, Pr-ion with n = 3–3.78 might mainly dominate PrO_x in the vicinity of GB. While in case of samples doped with Pr_6O_{11}, Pr-ion with n = 3.5–4 might mainly dominate PrO_x in vicinity of GB. In view of XRD results as listed in Table 1, the tendency seems to be much stronger in samples sintered in oxygen than in air.

Hence, we can consider that change in ρ of both OZP605 and OZP61 is obviously different from that of the others samples because of something originating in segregated PrO_x including Pr-ion with n = 3.5–4. Besides, samples including Pr-ion with n = 3–3.78 in vicinity of GB can show the maximum of ρ between 500 K and 667 K. Pr content dependence of the ρ increase at maximum supports this suggestion.

The appearance of ρ maximum

Except for both OZP605 and OZP61, the other doped samples show the maximum of ρ by 9th-cycle, although all samples sintered in air does not show at 2nd-cycle. The appearance of ρ maximum seems to relate with the concentration dependence of defects or the complex that can affect the electrical properties. As mentioned above, the origin of such defects or the complex should be related

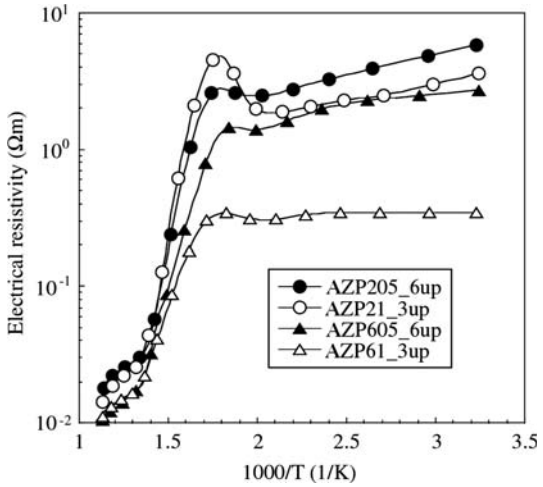

Fig. 6 The temperature dependence of ρ for AZP205 and AZP605 at 6th-cycle-heating and that for AZP21 and AZP61 at 3rd-cycle-heating

with Pr-ion in vicinity of GB. Figure 6 shows the temperature dependence of ρ for samples sintered in air at 3rd-cycle and 6th-cycle, where we can identify the initial appearance of ρ maximum. The Pr 0.5 mol% doped samples show the maximum at 6th-cycle, and the Pr 1 mol% doped samples show the maximum at 3rd-cycle. The appearance of ρ maximum depends on the Pr content in samples.

Chun et al., have suggested that both mass transport and the GB formation behaviors in ZnO–Pr–Co system ceramics are strongly affected by firing atmosphere and temperature; In N_2, large Pr segregates are shown on the surface of fired ZnO because large vaporization of ZnO is occurred at the surface. On the other hand, In O_2, small Pr segregates are shown on the surface of fired ZnO because large vaporization of Pr was occurred at the surface [39], where their samples were sintered at high temperature between 1473 K and 1773 K. Their experimental result supports that there is difference in the initial appearance of ρ maximum in our samples, that is, there is difference in the concentration of both Pr and the related-defect complexes originating in enhanced V_{Zn} with acceptor-like in vicinity of GB [17–20].

Hence, the concentration gradient governs the temperature dependence of ρ in cycles for each sample, where the change of ρ is stable against the change of temperature when the chemical reactions inside and outside the bulk are steady or in equilibrium.

Heat-treatment cycle dependence of ρ at 400 K

Figure 7 shows the heat-treatment cycle dependences of ρ at 400 K on heating process of samples doped with (a) Pr_2O_3 and (b) Pr_6O_{11}, respectively. In Fig. 7(a), ρ of all doping samples largely decrease at 3rd, and then the degree of decrease is smaller in 0.5 mol% doped samples than in 1 mol% doped samples. ρ of 0.5 mol% doped samples are steady from 3rd, while ρ of 1 mol% doped samples seem to be steady from 7th or 8th. In Fig. 7(b), ρ of both AZP605 and AZP61 largely decrease at 3rd, and then the degree of decrease is smaller in AZP605 than in AZP61. ρ of AZP605 are steady from 3rd, while ρ of AZP61 tends to decrease slightly. In contrast, ρ of both OZP605 and OZP61 tend to increase, and the degree of increase is much larger in OZP605 than in OZP61.

The specificity of both OZP605 and OZP61 as shown in Fig. 5 is also shown in Fig. 7(b). The dependence of ρ between Pr content and the heat-treatment cycle seems to be closely related with the dependence of ρ between the concentration gradient and the temperature as shown in Fig. 6. Hence, we can conclude that the appearance of ρ maximum seems to be closely related with Pr and the related-defect complex originating in V_{Zn} with acceptor-like in the vicinity of the GB in particular [17–20].

Thermoelectric properties

It was confirmed that the porous ZnO:Pr ceramics had the unique characteristic of the rho maximum with increasing temperature. The origin of ρ maximum seems to associate with the related-defect complexes originating in enhanced V_{Zn} by the Pr doing in ZnO. Assuming that the Pr doping affects the carrier transport in the vicinity of GB in particular, the thermo electric power might be also affected by the Pr doing. Figure 8(a) shows the temperature dependence of absolute value of α for AZN, OZN, OZP205, AZP21 and OZP21 at 9th-cycle-heating. The absolute value of α for AZN is the lowest in the whole temperature range in Fig. 8(a), and as shown in Fig. 4(a), ρ of AZN at 9th-cycle-heating is relatively lower compared with that of the other samples. On the other hand, the absolute value of α for OZP205 is higher than that for AZN in Fig. 8(a), although ρ of OZP205 at 9th-cycle-heaing in Fig. 3(b) is lower that that of AZN. The relationship between α and ρ for OZP205 is against the expression of thermoelectric power for the semiconductor generally expressed by

$$\alpha = \frac{k}{e}\left(\frac{5}{2} + \gamma + \ln\left\{\frac{2(2\pi mkT)^{3/2}}{nh^3}\right\}\right). \quad (1)$$

where k is the Boltzmann constant, γ is the $d(ln\ \tau)/d(ln\ E)$ as the scattering relaxation time of carrier τ, m is the effective mass of carrier, n is the density of carrier, and h is Plank constant [40]. The α is getting larger with lower density of carrier or heavier effective mass. Hence, in case of larger α for OZP205 in particular, it is considered that the enhanced related-defect complexes by the Pr doing and Pr itself let effective mass of carrier in the vicinity of GB to get heavy, or the result of combinations of the different phases.

Thermoelectric properties were often evaluated by using power factor $P(= \alpha^2 / \rho)$ which indicates the electrical power generation capability in common materials. As the result of thermoelectric measurements, OZP205 had the largest value of P in the whole range among all samples. Figure 8(b) shows the temperature dependence of P for AZN, OZN, OZP205, AZP21 and OZP21 at 9th-cycle-heating. In Fig. 8(b), P of OZP205 is one order of magnitude at 400 K larger than that of AZN and OZN, where the absolute value of α in the whole range is large in the order of OZN, OZP205, and AZN as shown in Fig. 8 (a). ρ of OZP205 is the lowest in the whole temperature range, and the degree of ρ change in the measurement temperature range is also the lowest among all samples as shown in

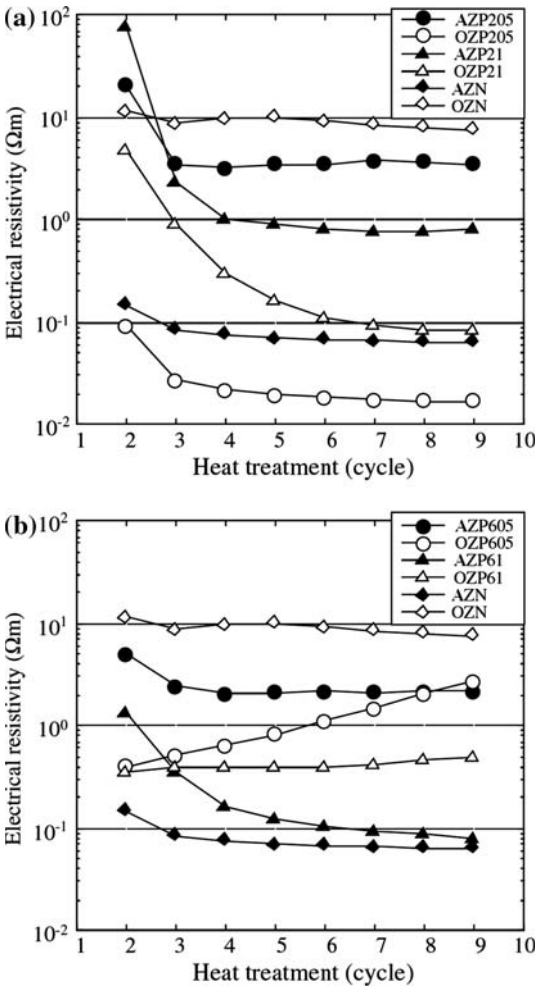

Fig. 7 The heat-treatment cycle dependence of ρ at 400 K on heating process of samples doped with (**a**) Pr_2O_3 and (**b**) Pr_6O_{11} in addition to non-doped samples as reference

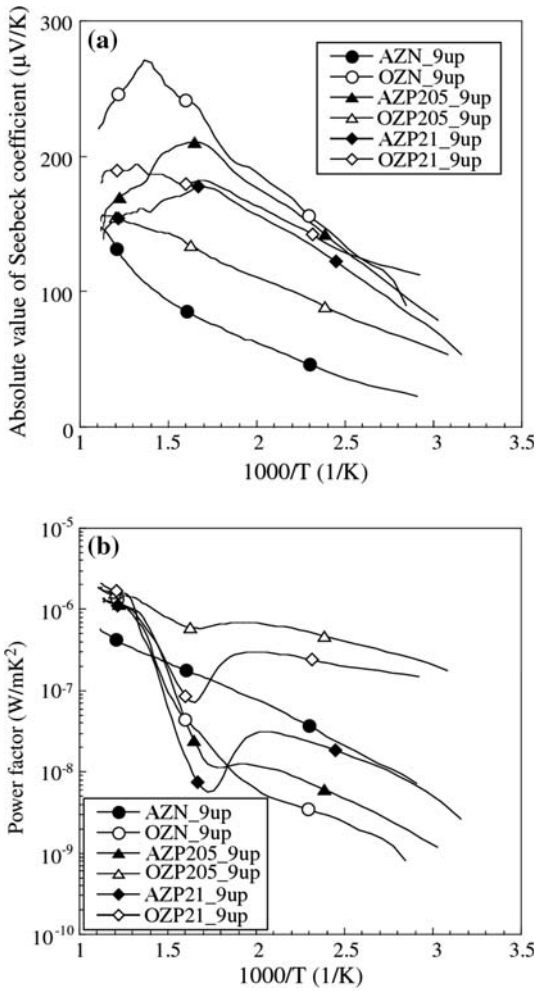

Fig. 8 (**a**) The temperature dependence of absolute value of α and (**b**) The temperature dependence of P for AZN, OZN, OZP205, AZP21 and OZP21 at 9th-cycle-heating

Fig. 3(b). Moreover, the low as well as stable ρ in the whole range is still obtained through the repeated heat-treatment measurement as shown in Fig. 7(a). This result for OZP205 about ρ is noticeable in view of thermoelectric properties improved. Because high P, low ρ and low thermal conductivity (κ) are required in order to achieve high performance on thermoelectric power. However, the value of P for OZP205 in this work is still poor for thermoelectric power. For example, $NaCo_2O_4$ shows $P = 50 \times 10^{-6}$ W/K^{2}cm at 300 K, and this P is comparable to a typical thermoelectric material such as Bi_2Te_3 [41].

It is important that the low ρ can be achieved at porous ZnO bulk doped with Pr 0.5 mol% as Pr_2O_3 additive. The doping of Pr into ZnO matrix seems to be very effective in view of modification for thermoelectric materials based on ZnO system if the doping condition can be controlled. Because Pr doping into ZnO matrix might brought about low κ, that is, a phonon scattering might occur at the vicinity of GB by point defects such as both Pr-ion and the related-defects complex. The further enhancement of high P as well as low ρ might be probably achieved by thinned amorphous film [40], and then such fabricated films might be prospective as one of thermoelectric materials used for infrared sensor and so on under severe condition.

On the other hand, Pr doped porous ZnO ceramics, in particular AZP21, obtained in this work show unique electrical property such as critical temperature coefficient (CTR) in temperature range between 588 K and 769 K. Hence, utilizing this property is expected to give great hope to gas sensor materials [42, 43].

Conclusion

The low density ceramics of porous ZnO doped with Pr (0.5 and 0.1 mol%) were prepared by sintering in air and

oxygen. Here, the additives were Pr_6O_{11} known for phase transformations and the trioxide Pr_2O_3 with low valence state. It was found that obtained all samples had the structure of ZnO lattice including a few Pr oxide crystal phase. Then, to evaluate effects of Pr doping for thermoelectric properties of samples, we measured ρ in temperature range between about 313 K and about 903 K. The temperature dependence of ρ for all samples except for OZP605 and OZP21 showed the maximum at higher temperature region around 590 K. The origin of maximum was studied on the basis of carrier transport model on gas sensor and varistor consisted of ZnO system. As the result, it was suggested that the maximum as well as the change of ρ was attributed to the interchange of carriers through defect complexes closely related with V_{Zn} acceptor-like electronic states in the vicinity of GB, where enhanced V_{Zn} seemed to be caused by Pr in PrO_x with valence state between 3+ and 3.78+ around GB. Then, the doping of Pr into ZnO matrix is advantageous to improve thermoelectric power.

Acknowledgements The authors would like to thank Professor Toshio Kawahara of Osaka University for helpful discussion.

References

1. Sato S, Miyayama M, Koumoto K, Yanagida H (1985) J Am Ceram Soc 68:40
2. Inaba R, Kajimura K, Mikoshiba N (1971) Jpn J Appl Phys 10:995
3. Mukae K, Tsuda K, Nagasawa I (1977) Jpn J Appl Phys 16:1361
4. Clarke DR (1999) J Am Ceram Soc 82:485
5. Tsukazaki A, Ohtomo A, Onuma T, Ohtani M, Makino T, Sumiya M, Ohtani K, Chichibu SF, Fuke S, Segawa Y, Ohno H, Koinuma H, Kawasaki M (2005) Nat Mater 4:42
6. Tsukazaki A, Kubota M, Ohtomo A, Onuma T, Ohtani K, Ohno H, Chichibu SF, Kawasaki M (2005) Jpn J Appl Phys 44:L643
7. Nishii J, Hossain FM, Takagi S, Aita T, Saikusa K, Ohmaki Y, Ohkubo I, Kishimoto S, Ohtomo A, Fukumura T, Matsukura F, Ohno Y, Koinuma H, Ohno H, Kawasaki M (2003) Jpn J Appl Phys 42:L347
8. Nishi J, Ohtomo A, Ohtani K, Ohno H, Kawasaki M (2005) Jpn J Appl Phys 44:L1193
9. Simpson JC, Cordaro JF (1988) J Appl Phys 63:1781
10. Santos JD, Longo E, Leite ER, Varela JA (1998) J Mater Res 13:1152
11. Inoue Y, Okamoto M, Kawahara T, Morimoto J (2005) Jpn J Appl Phys 44:4455
12. Cox SFJ, Davis EA, Cottrell SP, King PJC, Lord JS, Gil JM, Alberto HV, Vilão RC, Duarte JP, de Campos NA, Weidinger A, Lichti RL, Irvine SJC (2001) Phys Rev Lett 86:2601
13. Shimomura K, Nishiyama K, Kadono R (2002) Phys Rev Lett 89:255505-1
14. Kohan AF, Ceder G, Morgan D, Van de Walle CG (2000) Phys Rev B 61:15019
15. Oba F, Adachi H, Tanaka I (2000) J Mater Res 15:2167
16. Oba F, Nishitani SR, Isotani S, Adachi H, Tanaka I (2001) J Appl Phys 90:824
17. Oba F, Yamamoto T, Ikuhara Y, Tanaka I, Adachi H (2002) Mater Trans 43:1439
18. Oba F, Sato Y, Yamamoto T, Ikuhara Y, Sakuma T (2003) J Am Ceram Soc 86:1616
19. Sato Y, Mizoguchi T, Oba F, Yodogawa M, Yamamoto T, Ikuhara Y (2004) Appl Phys Lett 84:5311
20. Sato Y, Oba F, Yodogawa M, Yamamoto T, Ikuhara Y (2004) J Appl Phys 95:1258
21. Alles AB, Burdick VL (1991) J Appl Phys 70:6883
22. Yano Y, Takai Y, Morooka H (1994) J Mater Res 9:112
23. Mukae K, Ohi A, Tanaka A (2001) J Eur Ceram Soc 21:1871
24. Takata M, Tsubone D, Yanagida H (1976) J Am Ceram Soc 59:4
25. Fujitsu S, Toyoda H, Yanagida H (1987) J Am Ceram Soc 70:C-71
26. Burnham DA, Eyring L (1968) J Phys Chem 72:4415
27. Kang ZC, Eyring L (1997) J Alloy Compd 249:206
28. Tomimuro H, Terasaki Y (1979) Jpn J Appl Phys 18:1653
29. Anderson RA, Pike GE (2003) J Mater Res 18:994
30. Ohbuchi Y, Kimura A, Kawahara T, Okamoto Y, Morimoto J, Toyoda T (2001) Jpn J Appl Phys 40:3606
31. Ohbuchi Y, Kawahara T, Okamoto Y, Morimoto J (2002) Jpn J Appl Phys 41:190
32. Chen WP, Wang Y, Peng Z, Chan HLW (2003) Jpn J Appl Phys 42:L48
33. Chen WP, Chan HLW (2004) Jpn J Appl Phys 43:701
34. Sonder E, Austin M, Kinser DL (1983) J Appl Phys 54:3566
35. Lee Y-S, Liao K-S, Tseng T-Y (1996) J Am Ceram Soc 79:2379
36. Chun S-Y, Wakiya N, Funakubo H, Shinozaki K, Mizutani N (1997) J Am Ceram Soc 80:995
37. Wakiya N, Chun S-Y, Shinozuka K, Mizutani N (2000) J Solid State Chem 149:349
38. Ohashi N, Mitarai S, Fukunaga O, Tanaka J (1999) J Electroceram 4:S1:61
39. Chun S-Y, Mizutani N (2001) Mater Sci Eng B 79:1
40. Inoue Y, Okamoto M, Kawahara T, Okamoto Y, Morimoto J (2005) Mater Trans 46:1470
41. Terasaki I, Sasago Y, Uchinokura K (1997) Phys Rev B56:R12685
42. Lin F-C, Takao Y, Shimizu Y, Egashira M (1995) J Am Ceram Soc 78:2301
43. Agarwal G, Speyer R (1998) J Electrochem Soc 145:2920